ASIAN JOURNAL OF PHARMACEUTICAL AND CLINICAL RESEARCH

INNOVARE ACADEMIC SCIENCES
Knowledge to Innovation

Vol 18, Issue 10, 2025

Online - 2455-3891
Print - 0974-2441

Research Article

DESIGN, CHARACTERIZATION, AND EVALUATION OF CURCUMIN NANOSPONGES LOADED INTRAVAGINAL HYDROGEL FOR THE TREATMENT OF ENDOMETRIOSIS

ABHINIUMMANGAL BALAN[1], BHAVNA KUMAR[1]*, GURUSAMY MARIAPPAN[2]

[1]Faculty of Pharmacy, DIT University, Dehradun, Uttarakhand, India. [2]Department of Pharmaceutical Chemistry, St. Mary's College of Pharmacy, Secunderabad, Telangana, India.
*Corresponding author: Dr. Bhavna Kumar; E-mail: bhavna@dituniversity.edu.in

Received: 05 July 2025, Revised and Accepted: 25 August 2025

ABSTRACT

Objectives: This work aimed to optimize the process parameters for curcumin (CUR)-loaded nanosponges (NSs) and evaluating the prepared NSs hydrogel for the treatment of vaginal endometriosis.

Methods: The independent factors of CUR-loaded *β*-Cyclodextrin NSs (*β*CDNSs) production were optimized using Box–Behnken Design (BBD). CUR-*β*CDNSs were synthesized using lyophilization with carbonyldiimidazole as a cross-linking agent, and then formed into a hydrogel by the cold method. Experimental runs from a three-factor, three-level BBD were used in these studies.

Results: The mean particle size was 76.78–154.56 nm, and encapsulation effectiveness was 76.62–86.68%. Fourier transformed infrared, differential scanning calorimetry, and X-ray diffraction showed CUR-NSs inclusion complex development. Transmission electron microscopy revealed CUR in the polymer core. *In vitro* release tests showed NSs released 85% CUR in 120 min. Photostability and simulated intestinal fluid testing resulted in positive results. Free-CUR, CUR-*β*CDNSs, and ascorbic acid demonstrated antioxidant activity *in vitro* with SC50 values of 536.44, 187.48, and 81.16 µg/mL, respectively. This hydrogel's viscosity ranged from 6358 to 6879 cps, and its strength varied with temperature. The mucoadhesive strength was 1356.78–1487.29 N/m^2. *In vitro*, simulated fluid released 90% CUR in 60 min against 53% in citrate buffer. CUR-*β*CDNSs hydrogel demonstrated consistent CUR release in simulated vaginal fluid. Poloxamer-based CUR-*β*CDNSs hydrogels *in situ* gelling enhances bioavailability by forming a gel at higher temperatures and slowly releasing CUR.

Conclusion: The research recommended that CUR-*β*CDNSs hydrogel can be a good and efficient alternative for the treatment of endometriosis.

Keywords: Curcumin, Nanosponges, Hydrogel, Optimization, Endometriosis.

 DOI: http://dx.doi.org/10.22159/ajpcr.2025v18i10.55911. Journal homepage: https://innovareacademics.in/journals/index.php/ajpcr

INTRODUCTION

Endometriosis, a condition causing uterine tissue to grow outside the uterus, can cause infertility. CUR is believed to have antioxidant, anti-inflammatory, antimutagenic, antiviral, antifungal, and anticarcinogenic effects [1]. It reduces estrogen levels in endometriosis, but traditional methods are ineffective. Advanced delivery methods are needed to address the underlying causes rather than the symptoms, like pain [2]. Multiple studies have demonstrated that nanosponges (NSs) can enhance the bioavailability and targeting of medications [3]. The sponge operates as a three-dimensional framework or structure. Resulting in spherical particles with hollow spaces for drug molecules [4].

The*β*-Cyclodextrin-based NSs (*β*-CDNSs) provide a new carrier system that has the potential to greatly improve the effectiveness of drug formulations [5]. The *β*-CDNSs, a promising class of cross-linked polymers with unique three-dimensional structures, are being studied for their potential in vaginal medication delivery due to their effective containment of bioactive substances.

Drugs can be administered through the vagina in various dosage forms such as tablets, creams, gels, pessaries, foams, ointments, films, tampons, vaginal rings, and douches. Hydrogels, hydrophilic polymeric networks, are user-friendly and exhibit biological tissue qualities while maintaining mechanical integrity, making them a preferred option for aqueous environments. Currently, *in situ*-gelling liquids have also demonstrated their convenience as dosage forms for local applications due to their ease of administration into specific body cavities, which may then transform into a gel. The study proposes integrating CUR-loaded NSs into a temperature-sensitive hydrogel by optimizing process parameters through experiment design [6]. Response Surface Methodology, a statistical approach, is employed to build DoE and construct experimental models that connect several interacting components [7]. Box–Behnken designs (BBD) are the most commonly employed designs in response surface modeling. The current work utilized a three-level definitive screening design (DSD) to examine the impact of four independent parameters, including reaction temperature, reaction duration, stirring speed, and volume of solvent, on two responses: encapsulation efficiency (EE) and particle size of NSs [8-10]. The study aimed to improve CUR targeting efficacy by integrating it with NSs, optimizing settings, characterizing, and evaluating the potential use of CUR-loaded NSs hydrogel for the treatment of vaginal endometriosis.

MATERIALS AND METHODS

Materials

β-CD was obtained as a gift sample from Gangwal Chemicals Pvt. Ltd., Mumbai, India. Carbonyldiimidazole, Poloxamer-407, Poloxamer-188, and 2, 2-Diphenyl-1-picrylhydrazyl (DPPH) were purchased from Sigma Aldrich, MO, USA. Dimethyl sulfoxide, ethanol, methanol, sodium lauryl sulfate, hydroxypropyl methyl cellulose, citric acid, and sodium citrate were obtained from S.D. Fine Chemicals, Hyderabad, India. The curcumin (CUR) was purchased from NatuRite™ Agro Products Ltd., Hyderabad, India. For *in vivo* studies, New Zealand, White rabbits and BALB/c mice were procured from Gentox Bio Services Pvt. Ltd., Hyderabad, India, and maintained under standard laboratory conditions. Data analysis and statistical evaluations were performed using GraphPad Prism Version 6.0 (GraphPad Software Inc., San Diego, CA, USA).

Instruments

In the present study, a comprehensive range of instruments and analytical tools was employed. Lyophilization of the formulations was carried out using a FreeZone 6 Liter Freeze Dryer (Labconco Corp., Missouri, USA). Mechanical agitation during experimental procedures

was facilitated by a Remi Orbital Shaker (Remi Equipments, India), while centrifugation was performed using a Remi C-24 Plus High-Speed Cooling Centrifuge (Remi Equipments, India). UV absorbance measurements were obtained with a Shimadzu UV-1800 UV–Visible spectrophotometer (Japan). Particle size distribution was analyzed using a Mastersizer 2000 Laser Diffraction Particle Size Analyzer (Malvern Instruments Ltd., Worcestershire, UK), and ultrastructural analysis was conducted by transmission electron microscopy (JEM-2000 EXII; JEOL, Tokyo, Japan). Fourier-transform infrared (FTIR) spectra were recorded using a Tensor 27 FTIR Spectrophotometer (Bruker Optics, Germany), while thermal behavior was assessed with a Shimadzu DSC-60 Differential Scanning Calorimeter (Japan). X-ray diffraction studies were performed on a Bruker D8 Advance X-ray Diffractometer (Germany). Dialysis experiments were carried out using a Sartorius Dialysis Membrane (MWCO: 12 kDa, Germany). Photodegradation studies were conducted using a UV Lamp (VilberLourmat, France) emitting light in the 320–400 nm range. Viscosity was measured by a Brookfield Digital Viscometer DV-II+ Pro with LV spindle set (Brookfield Engineering, USA). *Ex vivo* permeation studies were performed using a Franz Diffusion Cell (PermeGear, USA). Stability testing was carried out in an International Council for Harmonization (ICH)-compliant Stability Chamber (Labindia, India). Chromatographic analysis was performed on a Waters Alliance e2695 high-performance liquid chromatography (HPLC) system equipped with a 2998 PDA detector and Breeze software (Waters Corp., Milford, MA, USA).

Experimental design

The objective of the experiment was to determine an optimal combination of the four variables (reaction temperature, reaction duration, stirring speed, and volume of solvent) that increases the effectiveness of encapsulation while simultaneously minimizing the particle size. Three coded levels (−1, 0, and +1) were chosen for each component, representing a range of values relevant to practical applications. The DSD matrix was constructed using Design Expert® V-13.0.9.0 software developed by Stat-Ease, Inc. in Minneapolis. The CUR-NSs were optimized using BBD software, with three distinct factors (independent variables) such as stirring speed (A), stirring duration (B), and volume of solvent (C). The BBD with three elements at three levels was utilized to optimize and assess the primary, interaction, and quadratic impacts of influential variables on response parameters. The BBD was suitable for constructing second-order polynomial models and describing quadratic response surfaces [3].

Data analysis of design

A variety of statistical characteristics, such as the model p-value, p-value of lack of fit, Regression coefficient (R^2), adjusted R^2, and coefficient of variation, were taken into account to choose the most appropriate and accurate model. Typically, model terms with a p-value larger than 0.005 are deemed inconsequential and can be removed from the model. The response parameter may be assessed using a quadratic model by the application of multiple regression analysis, as demonstrated by Eq. 1.

$$Y = \beta_0 + \beta_1 X_1 + \beta_2 X_2 + \beta_3 X_3 + \beta_{12} X_1 X_2 + \beta_{23} X_2 X_3 + \beta_{13} X_1 X_3 + \beta_{11} X_1^2 + \beta_{22} X_2^2 + \beta_{33} X_3^2 \quad (1)$$

Where, Y = Response parameter, β_0 = Intercept, β_1–β_3 = Regression coefficients, β_{12}, β_{13} and β_{23} = Interaction coefficients, β_{11}, β_{22} and β_{33} = Quadratic coefficients, X_1, X_2 and X_3 = Main influencing factors, X_1X_2 = Interactive effect and X_1^2, $X_2^2$and X_3^2 = Quadratic effect.

The backward elimination approach removes non-significant independent variables from the regression equation, while three-dimensional response surface plots and perturbation and contour plots illustrate the functional correlation [11].

Synthesis of NSs

The *β*-CDNSs were synthesized utilizing carbonyldiimidazole as the crosslinking agent, following published protocols [12]. The reactions were carried out with meticulous accuracy, ensuring stringent temperature regulation by the use of a constant-temperature oil bath. In a 250 mL flask, 1.134 g (0.001 mol) of anhydrous *β*-CD was dissolved in dimethyl sulfoxide. A quantity of 2.484 g of carbonyldiimidazole was introduced into the reaction mixture and subjected to reflux in an oil bath. The resulting product was rinsed with Milli-Q water and then purified by Soxhlet extraction using ethanol for 4 h. The resultant white product was dried at 60°C in powder form and then pulverized using a mortar and pestle. The finely ground substance was reconstituted in Milli-Q water. The suspended colloidal component in water was retrieved using lyophilization, which involved subjecting it to temperatures of −50°C and a pressure of 0.02 m Barusing a FreeZone-6 L Lyophilizer (Labconco Corp., MO, USA).

Solubilization efficiency of NSs

The solubilization efficacy of NSs toward CUR was examined to assess their ability to enhance solubility, as shown in a previous study [13]. Around 1000 mg of CUR was mixed with 100 mg of NSs in 10 mL of Milli-Q water. The volumetric flasks were positioned on a mechanical shaker at room temperature. Following a 24 h period of equilibrium, the suspension was subjected to centrifugation for 10 min at 10,000 rpm. This process allowed for the separation of the unbound CUR, while the resulting colloidal supernatant was collected. An additional 10 mL of methanol was introduced to the supernatant to extract the CUR that was enclosed within the NSs. The solution was subsequently examined using a UV-spectrophotometer. The study enabled us to measure the amount of drug present in the colloidal supernatant, giving us valuable information about the increased solubility attained by different formulations.

Characterization of plain *β*-CDNSs and CUR-NSs

Particle size, polydispersity-index, and zeta-potential

The dynamic light scattering technique was used to investigate the particle size distribution. The measurements were performed with a Mastersizer-2000 device manufactured by Malvern Instruments Ltd, located in Worcestershire, UK. The measurements were taken at a fixed angle of 90°. The samples were diluted with Milli-Q water for accuracy, and zeta potential measurements were carried out by the same instrument temperature of 25±2°C.

Drug payload (%DL) and %EE

EE measures the proportion of the drug's weight enclosed within the carrier system compared to the original drug amount. Drug loading is defined as the proportion of the drug's mass to the total mass of the carrier system. To obtain these essential parameters, a certain amount of CUR-loaded NSs complexes was initially dissolved in methanol, followed by sonication. The solution obtained was suitably diluted and thereafter analyzed using a UV/Vis spectrophotometer at 425 nm. The drug payload and EE were calculated using the following equations (Eq. 2 and Eq. 3, respectively) [14].

$$\%DL = \frac{Weight\ of\ CUR\ encapsulated\ in\ NSs}{Weight\ of\ the\ NSs\ taken\ for\ analysis} \times 100 \quad (2)$$

$$\%EE = \frac{Weight\ of\ CUR\ encapsulated\ in\ NSs}{Initial\ weight\ of\ CUR\ fed\ for\ loading} \times 100 \quad (3)$$

Transmission electron microscopy (TEM)

A transmission electron microscope (JEM-2000 EXII; JEOL, Tokyo, Japan) was used to study the structure of CUR-loaded NSs. A diluted NS solution was applied to a copper grid coated with a thin coating, subjected to phosphotungstic acid, dried, and examined using transmission electron microscopy at 30,000× magnification. The research yields useful insights into the morphology and structural aspects of the NS complexes [15].

FTIR spectroscopy

The Tensor 27 FTIR Spectrophotometer was used to study CUR-loaded NSs. The potassium bromide (KBr) pellet method was employed to prepare the sample, and scanned from 400 cm^{-1} to 4000 cm^{-1} wavenumber.

Differential scanning calorimetry (DSC)
The equipment underwent calibration using indium to determine its melting point and heat of fusion. A heating rate of 10°C/min was used to increase the temperature from 30°C to 400°C. Aluminum sample pans were utilized, with an empty pan serving as the reference. The analyses were conducted in triplicate on 5 mg samples under a nitrogen purge.

X-ray diffraction (XRD) study
The investigations were conducted with a Bruker D8 Advance X-ray diffractometer, a very effective instrument for examining the crystalline properties of materials. For the XRD study, a scan rate of 5°/min was used to thoroughly cover the 2θ range from 2.5° to 60°.

***In vitro* release study**
The *in vitro* release investigation was conducted utilizing multi-compartment (n=3) rotating cells equipped with a dialysis membrane (Sartorius MWCO: 12kDa). The donor phase contained 1 mL of 1 mg/mL of CUR-loaded formulations, where phosphate buffer saline (pH 7.4) was used as suspending medium. The CUR suspension was prepared by suspending a weighed amount of CUR to get 1 mg/mL CUR strength in an aqueous solution of sodium carboxymethyl cellulose as suspending agent (5%, w/v), PEG-400 as wetting agent (5%, w/v), and βCD as solubilizing agent (10%, w/v). The receptor phase similarly comprises the identical media. In the release medium, 1 mL of 0.5% (w/v) sodium lauryl sulfate solution was added to the receptor phase to enhance the solubilization of CUR in an aqueous environment. The receptor phase was entirely removed at regular time intervals, appropriately diluted with distilled water, and examined by a UV-spectrophotometer at 425 nm [16].

Photodegradation study
The photodegradation study was conducted with a UV lamp emitting light within the wavelength range of 320–400 nm. The investigated systems consisted of aqueous suspensions containing unmodified CUR and CUR-loaded NSs. A 10 mL portion of each system was positioned 10 cm away from the light source and exposed to radiation while continuously stirring. At intervals of 30 min, a total of 3 h of irradiation, fixed volumes (200 µL) of each sample were extracted and diluted 1:10 (v/v) with methanol for spectrophotometric analysis [17].

Stability assay at pH 7.4 in phosphate buffer
The stability of CUR, both in its free form and when entrapped in the structure of NSs, was examined in phosphate buffer (pH 7.4) at 37°C throughout 24 h. Around 5 mg of each sample was added to phosphate buffer in different 50 mL centrifuge tubes, and incubated at 37°C. At regular time intervals of 0, 1, 2, 4, 6, 12, and 24 h, around 2 mL samples were taken, extracted, and examined at 425 nm by a UV-spectrophotometer[18].

Antioxidant activity by DPPH
The antioxidant efficacy of CUR was assessed using the DPPH scavenging activity method. The scavenging effect (%) was calculated using the following equation (Eq. 4). Thereafter, the scavenging concentration at 50% (SC_{50}) was used to compare the scavenging activity.

$$Scavenging\,effect\,(\%) = \frac{A_{Control} - A_{Sample}}{A_{Control}} \times 100 \quad (4)$$

Development of vaginal *in situ* hydrogel
The thermosensitive *in situ* hydrogels were prepared by following the cold technique. The detailed description of the formulations with ingredients and the compositions is summarized in Table 1. The hydroxypropyl methylcellulose (HPMC) grade K4M was slowly introduced into a citrate buffer (pH 4.5) while being stirred at 1000 rpm at 4°C until completely dissolved, followed by the addition of Poloxamer-407 and Poloxamer-188. The obtained polymeric solution was refrigerated for a minimum of 24 h to guarantee full dissolution.

Table 1: Formulation of hydrogels with ingredients and their compositions.

Ingredients	Compositions for	
	CUR-βCDNSs hydrogel	Free CUR-hydrogel
CUR-loaded βCD-NSs(≈ 100 mg CUR)	260 mg	100 mg (CUR only)
Poloxamer-407	20% w/v	20% w/v
Poloxamer-188	5% w/v	5% w/v
Hydroxypropyl methylcellulose (K4M)	1% w/v	1% w/v

CUR: Curcumin, NS: Nanosponges, βCD: β-Cyclodextrin

Around 100 mg of CUR was suspended in 2 mL of absolute ethanol. Then, 2 mL of this CUR suspension was added to 8 mL of the previously prepared polymeric solution to get pure-CUR hydrogel. The resulting mixture was refrigerated at 4°C for 48 h to eliminate foam and allow the gel to stabilize.

Evaluation of *in situ* hydrogel
Gelation temperature, pH, and viscosity
Formulation in sol state (10 mL) was agitated using a magnetic stirrer at 25°C. The solution was subjected to uniform heating at a rate of 1°C/min. The process involved the consistent agitation of the mixture at a speed of 200 rpm using a magnetic bead. The temperature at which the magnetic bead ceased motion as a result of gelation was documented as the gelation temperature (T_{gel}). The dilution was performed at a ratio of 10:3.7 (v/v) using a citrate buffer of pH 4.5. The T_{gel} was then determined using the same approach. The pH of the solution was determined using a digital pH meter. The viscosity of the *in situ* hydrogel was determined by a Brookfield viscometer with LVDV Spindle Number-96. The viscosity was assessed at three distinct temperatures (4°C, 25°C, and 37°C) to examine the impact of temperature on viscosity, while also considering the influence of flow. The viscosity was determined at 20 rpm, 50 rpm, and 100 rpm.

Mucoadhesive strength
The mucoadhesive force of the formulations was assessed by quantifying the force necessary to separate the formulation from a mucosal membrane, specifically, goat vaginal mucosa. The lower surface of the redesigned balance was affixed horizontally with a vaginal mucosa. Before the mucoadhesion test, the vaginal mucosa was moistened with warm citrate buffers (37°C; pH 4.5). Three droplets of the solution were applied onto the top of an inverted beaker, and the liquid sample that formed in that location was subjected to a heat source to induce gelation. The elevated section of the altered equilibrium apparatus, which includes the moisturized membrane, was aligned to make direct contact with the prepared solution. To establish a strong adhesive connection, a preload of 10 g was promptly provided for 1 min, ensuring close contact between the membrane and the sample. Once the preload time was over, water was poured into a plastic jar that had been weighed beforehand. The jar was put on the left pan of the balance, and water was supplied at a consistent rate of 5 mL/min. The water addition was halted on detachment of the membrane from the tested sample. Subsequently, the filled plastic jar was reweighed, and the amount of water needed to detach the tested sample from the vaginal mucosal membrane was determined using Eq. 5.

$$Detachment\,stress = \frac{mg}{A} \quad (5)$$

Gel strength
The experiment involved diluting the *in situ* hydrogel with citrate buffer (pH 4.5) at 10:3.7 (v/v) ratio. The resulting mixture was then transferred to a 100 mL graduated cylinder. Gelation was initiated by maintaining a temperature of 37°C. A disc weighing 1 g, having a diameter of 1.5 cm, was placed on the surface of the gelled formulation inside the cylinder.

Different weights were then added on top of the apparatus. The gel strength was determined by measuring the minimum weight required to push the apparatus down 5 cm into the sample.

***In vitro* drug release**

A volume of 2 mL of formulation was added to a Petri dish containing 10 mL of citrate buffer (pH 4.5). The Petri dish was securely sealed and positioned on a shaker operating at 37°C with low speed. The eluates from the hydrogel were extracted from each Petri dish at 10-min intervals, and the volume of each Petri dish was refilled with 10 mL of fresh release medium. The quantities of CUR in the eluates from the hydrogel were quantified at 425 nm by a UV-spectrophotometer. This experiment was performed to investigate the breakdown of hydrogel-based formulation in a fluid that mimics the conditions of the vagina, known as vaginal simulant fluid (VSF). The VSF was prepared as per the available literatures [19].

Stability study

Stability studies were conducted according to the ICH guidelines. The optimized formulation was placed in 50 mL white low-density polyethylene plastic bottles and stored in a stability chamber at a set temperature of 25±2°C for 3 months. The chemical stability of formulations was determined by measuring the drug assay in the formulation. Physical stability was tested by monitoring changes in pH, gelation temperature, mucoadhesive strength, gel strength, viscosity, and appearance.

***Ex vivo* skin permeation study**

The Franz diffusion cell was also used to conduct the *ex vivo* skin permeation investigations on rat skin. The skin specimens were placed between the donor and receptor compartments of the diffusion cell (cross-sectional area of 1.62 cm^2) in such a way that the epithelial layer was facing the donor phase. The equivalent amounts of CUR-NSs hydrogel (CUR-βCDNSs) and free-CUR in hydrogel (each containing 62.5 mg of CUR) were placed on the epithelial surface of the skin in the donor compartment. The receptor compartment was filled with 12.5 mL of citrate buffer (pH 4.5). Throughout the experiment, the temperature was kept at 37±1°C. Samples from the receptor compartment were obtained at different time intervals to measure the amount of CUR that penetrated the animal's skin. The collected samples were subjected to spectrophotometric analysis at 425 nm to determine the drug concentration.

***In vivo* pharmacokinetic (PK) analysis**

A total of six New Zealand rabbits of both sexes, weighing 2–2.5 kg (n=12), were used for *in vivo* PK studies. The animals were provided with a standard diet and water for one week before the procedure. The Institutional Animal Ethical Committee (IAEC No. 1447/PO/Re/S/11/CPCSEA-65/A) approved experimental protocols for the animal studies.

Before the day of drug administration, rabbits were fasted overnight but were allowed access to water. Three rabbits were given oral doses of CUR-suspension (62.5mg in 0.1% CMC). The abdominal hair of the other three rabbits was shaved for transdermal application of the gel. Before applying the transdermal gel (CUR-βCD-NSs or CUR-NSs hydrogel), the skin was gently wiped with warm water, followed by an alcohol swab, and patted dry. An equivalent amount of CUR-NSs hydrogel (containing ≈ 62.5 mg of CUR) was applied to the shaved skin covering around a 4 × 4 cm^2 area. The oral dose of CUR was decided on the basis of previous reports [20]. The blood samples of approximately 0.5 mL were collected from the jugular vein in dried heparinized tubes at regular intervals after oral and transdermal administration. The plasma was separated, and 100 µL of supernatant was collected in Eppendorf tubes and stored at −20°C until analysis.

PK sample analysis

The reported HPLC method, photo diode array detector (PDA), was used for the analysis of CUR in plasma samples. Briefly, around 500 µL of a 95:5 (v/v) mixture of ethyl acetate and methanol was added to each sample (standards and unknowns) as an extraction reagent. The mixture was centrifuged at 13000 rpm for 5 min. After centrifugation, 300 µL of the supernatant was collected into new 500 µL capacity microcentrifuge tubes and dried under a nitrogen stream. The dried samples were suspended in 250 µL of the mobile phase mixture. After vortexing for 30 s, the samples were kept in the dark for 15 min at ambient temperature. Thereafter, the samples were vortexed again and transferred into sample vials. A 20 µL of content was injected into the column for chromatographic separation of CUR.

The Waters® (USA) HPLC system with PDA-detector at 425 nm was used for the processing of the samples. The system was equipped with "Breeze software" (Waters®, USA) for the integration of the results and data. A reverse-phase C_{18} Column (Macherey-Nagel, 150 × 4.6 mm, 5 µm) was used for the chromatographic separation and elution of CUR.A (v/v) mixture of acetonitrile: methanol: water: acetic acid (40:24:35:1) was pumped at 1 mL/min (flow rate) as the mobile phase, and the volume of injection was 20 µL. The concentration of CUR was determined using a calibration curve generated by spiking eight plasma samples (200 µL each) with different amounts of CUR stock solution (200 µg/mL) to get the concentration range 2–10 µg/mL of CUR.

After sample analysis, the CUR plasma concentration versus time plots was generated. The non-compartmental approach was used to calculate the PK parameters using PK-Solver (an Add-in program for PK data analysis) in Microsoft Excel 2016 [21]. The area under the CUR concentration-time curve (AUC) measures the total amount of CUR present in blood. The important PK parameters such as the maximum plasma concentration (C_{max}, ng/mL), time to achieve the maximum plasma concentration ($T_{max,}$ h), elimination half-life ($t_{1/2}$, h), area under curve from 0 to 24 h ($AUC_{0\text{-}24h}$, ng.h/mL), and 0-infinity ($AUC_{0\text{-}inf}$, ng.h/mL) were calculated.

Evaluation of anti-endometriosis activity of CUR-NSs as a nanogel in a mouse model

Induction of peritoneal endometriosis in BALB/c mice

Animal experiments were carried out following the guidelines of the Animal Ethics Committee of the Institute (MGI/IAEC/06/2023, Muppandal Genomics and Immunological Pvt. Ltd., Hyderabad, India). Induction of peritoneal endometriosis was carried out by previously reported methods with minor modifications [22].

A total of 30 female adult BALB/c mice, 6–8 weeks old, were used for these experiments. They were divided into five groups, each with six animals (n=6). Group-1 was for the normal control, Group-2 for endometriosis control, Group-3 for normal gel (CUR-hydrogel), Group-4 for CUR-βCD-NSs hydrogel (CUR-NSs Gel), and Group-5 for standard drug danozol. On the first day, donor mice were anesthetized with ketamine and sacrificed to obtain uterine horns under sterile conditions. The endometrium was extracted, chopped, suspended in sterile PBS, and inoculated into the peritoneal cavity of recipient mice. The animals were subjected to a 14-day drug treatment period, except for the normal control group. The normal control mice were administered only PBS (pH 7.4). No endometrial fragments were administered. Endometriosis control was monitored for 14 days using PBS, with normal gel 6 mg, CUR-NSs Gel 60 mg, and standard drug danozol (100mg/kg.bw) administered through the intravaginal route. The drugs were administered by the intravaginal route for 15 days to test their protective effects against endometriosis, with the uterus tissue collected and processed for further analysis.

Histopathological examination

The endometrial tissue samples from all groups (treated and control groups) were processed and stained with hematoxylin-eosin by routine procedures for the histopathological examinations [23].

Data analysis

Data were analyzed statistically by one-way analysis of variance (ANOVA) using GraphPad Prism V-6.0 Software (San Diego, CA, USA)

to evaluate the differences between the involved groups. The results were represented as the mean of three measurements with standard deviations (mean ± SD), unless indicated, such as the PK results, which were presented as the mean of six measurements with standard error of means (mean ± SEM). The level of significance was assumed significant at $p<0.05$.

RESULTS AND DISCUSSION

Optimization of reaction conditions

The study analyzed NSs synthesis by examining factors such as reaction temperature, duration, stirring speed, and solvent volume, finding that temperatures above 110°C resulted in a reticulate structure. The study demonstrates the production of *β*-CDNSs with varying particle sizes, optimizing parameters such as reaction temperature, stirring velocity, and solvent quantity for increased yield and narrow particle size distribution. The experimental design consisted of 13 runs, executed randomly to minimize uncontrolled variables, and determined using the equation (2k+3=13). Factors were tested five times at various levels, with three central values executed at each alternate factor's low, high, and center levels, resulting in extra replicates of the Center Point. The DSD and experimental data of responses with the actual values of factors are mentioned in Table 2.

Synthesis and solubility analysis of *β*-CDNSs

The*β*-CDNS offer regulated release, compatibility with living organisms, and natural breakdown. They can be manufactured by replacing hydrogen atoms on the outer surface of the original *β*-CD molecule. The study demonstrates a chemical modification that increases drug loading capacity in nano-channels of NS structures, enhancing their ability to dissolve substances and provide protection by facilitating interactions between guest molecules and numerous *β*-CD units. The approach of synthesizing NSs utilizing carbonyldiimidazole in a solution at elevated temperatures is a well-established method. The study investigated the solubility of CUR in distilled water and showed that it dissolved significantly on NSs at a concentration of 112 μg/mL.

Preparation of CUR-loaded NSs

Using the freeze-drying method, CUR was added to NSs [24]. The loading efficiency was determined to be 37.78% (w/w). The different CUR loading showed that the complexation capability of NSs was dependent on the degree of cross-linking and process parameters.

Optimization of CUR-loaded NSs

A total of 17 model experiments were arranged at random using the BBD model. The dependent variables (factors) and the relative responses are represented in Table 3 after the tests were conducted following the suggestions given by the BBD software.

The most significant factors influencing the performance metrics of *β*-CDNSs, including mean particle size and EE, were found to be the stirring speed, stirring duration, and solvent amount.

Table 2: Definitive screening design and experimental data of responses

Runs	Factors				Responses (Mean±SD, n=3)	
	A: Reaction temperature (°C)	B: Reaction time (min)	C: Stirring speed (rpm)	D: Volume of solvent (mL)	Practical yield (%)	Particle size (nm)
1	90	480	3000	125	82.52±4.21	234.84±10.57
2	80	480	4000	100	78.18±3.95	162.78±8.45
3	100	540	4000	100	85.08±4.05	142.89±10.06
4	90	420	2000	100	91.58±3.98	301.56±10.55
5	100	420	3000	100	83.18±2.87	170.82±8.09
6	100	420	4000	150	83.56±3.55	138.12±7.95
7	80	420	4000	125	75.12±7.86	164.12±8.75
8	100	480	2000	150	83.22±6.85	356.78±10.89
9	90	540	4000	150	95.42±9.01	138.12±9.85
10	80	420	2000	150	73.56±5.24	341.89±14.05
11	80	540	3000	150	77.84±3.57	212.34±11.56
12	100	540	2000	125	82.24±5.08	362.72±13.42
13	80	540	2000	100	76.54±4.85	348.34±12.05

All the values were expressed in (n=3), Mean±SD

Table 3: Data of definitive screening design and relative responses

Runs	Factors			Responses	
	A: Stirring speed (rpm)	B: Stirring time (h)	C: Volume of solvent (mL)	Y_1: Particle size (nm)	Y_2; Encapsulation efficiency (%EE)
1	4000	48	150	96.46	83.86
2	4000	24	150	110.34	81.82
3	3000	36	150	94.12	84.52
4	4000	36	200	107.78	79.56
5	2000	48	150	124.72	81.22
6	3000	36	150	93.48	83.92
7	3000	36	150	95.26	84.21
8	2000	36	200	144.12	76.62
9	2000	36	100	133.48	81.16
10	2000	24	150	154.56	79.34
11	3000	36	150	93.28	84.78
12	4000	36	100	99.12	82.12
13	3000	48	100	76.78	86.68
14	3000	24	200	108.56	81.12
15	3000	48	200	88.12	83.42
16	3000	24	100	101.44	83.89
17	3000	36	150	94.74	83.66

The studies determined the range of stirring speed (2000–4000 rpm), stirring time (24–48 h), and volume of solvent (100–200 mL). Based on the preliminary results, the BBD was used for the optimization of the factors that have an impact on the responses [25].

Seventeen trials were conducted according to a three-factor, three-level BBD. The average particle size (Y_1) ranged from 76.78 nm to 154.56 nm. The EE (Y_2) ranged from 76.62% to 86.68%. RSM approaches often aim to decrease the number of experimental runs and evaluate the interaction effects among chosen variables. The collected data were examined to get the ANOVA values, regression coefficients, and regression equation. The data were included in a second-order quadratic model, and the suitability of the model was verified by analysis of variance, lack of fit analysis, and the regression coefficient (R^2) values. The quadratic models with the greatest F-value were identified as the best-fitting models, as shown in Tables 4 and 5.

The mathematical equations for all three response variables were derived using multiple linear regression analysis and are displayed in Table 5. The coefficients of individual independent variables indicate their impact on response variables, with positive coefficients indicating synergy and negative coefficients indicating antagonistic effects. The regression equations were statistically significant, indicating the model's efficiency, while all quadratic models showed an insignificant lack of fit, indicating their adequacy. The multiple regression analysis shows R^2 values, corrected R^2 values, and coefficient of variation for all models. Both response parameters had R^2 values exceeding 0.98, indicating model suitability. However, a higher R^2 number does not guarantee soundness, so a modified R^2 value is crucial.

Particle size

The distribution of particle sizes has a significant impact on stability, solubility, dissolution, and the capacity to permeate various tissues and organs, especially in the context of targeted drug administration [26]. The particle size of the nano formulation varies between 76.78 and 154.56 nm. The model's F-value of 1545.03 indicates statistical significance, with $p<0.05$. Key terms include A, B, C, AB, BC, and A^2. Model reduction can enhance the model if irrelevant terms are removed. The F-value of 0.35 for lack of fit is not statistically significant, suggesting good model fit. The predicted R^2 value is close to the adjusted R^2 value, indicating <0.2 differences. Ades precision, a ratio of signal strength to background noise, is over 4, indicating a sufficient signal. The independent variables A and B have detrimental impacts, while factor C has favorable effects on particle size.

The individual impacts of A, B, and C on particle size were illustrated in the individual effects plot (Fig. 1a) and perturbation plot (Fig. 1b), allowing for a comparison between the expected and observed values. Figures 2 and 3 demonstrate the combined impact of independent factors on the particle size.

EE

The EE of NSs ranged from 76.62% to 86.68%. The model's F-value of 56.80 indicates statistical significance, with p-values below 0.0500 indicating the main terms are statistically significant, while values beyond 0.1000 suggest a lack of significance. The design space is navigated using a paradigm with a signal sufficient based on a ratio of 30.368, with variables A and B positively influencing efficiency. The contrast between the anticipated and actual values of particle size was

Table 4: Analysis of variance of the quadratic model: Mean particle size (nm)

Source	Sum of Squares	DF	Mean Square	F-value	p-value	
Model	6964.18	9	773.80	1545.03	<0.0001	significant
A: Stirring speed	2562.56	1	2562.56	5116.62	<0.0001	
B: Stirring time	986.12	1	986.12	1968.97	<0.0001	
C: Volume of solvent	178.23	1	178.23	355.86	<0.0001	
AB	63.68	1	63.68	127.15	<0.0001	
AC	0.9801	1	0.9801	1.96	0.2046	
BC	4.45	1	4.45	8.89	0.0205	
A^2	3154.64	1	3154.64	6298.80	<0.0001	
B^2	0.0033	1	0.0033	0.0066	0.9376	
C^2	0.7534	1	0.7534	1.50	0.2597	
Residual	3.51	7	0.5008			
Lack of Fit	0.7223	3	0.2408	0.3460	0.7951	Not significant
Pure Error	2.78	4	0.6959			
Corrected total sum of squares	6967.69	16				

Table 5: Analysis of variance of the quadratic model: Encapsulation efficiency (%EE)

Source	Sum of Squares	DF	Mean Square	F-value	p-value	
Model	95.49	9	10.61	56.80	<0.0001	Significant
A: Stirring speed	10.17	1	10.17	54.45	0.0002	
B: Stirring time	10.15	1	10.15	54.32	0.0002	
C: Volume of solvent	21.55	1	21.55	115.37	<0.0001	
AB	0.0064	1	0.0064	0.0343	0.8584	
AC	0.9801	1	0.9801	5.25	0.0558	
BC	0.0600	1	0.0600	0.3213	0.5885	
A^2	45.44	1	45.44	243.28	<0.0001	
B^2	1.66	1	1.66	8.87	0.0206	
C^2	4.80	1	4.80	25.70	0.0014	
Residual	1.31	7	0.1868			
Lack of Fit	0.5003	3	0.1668	0.8263	0.5442	Not significant
Pure Error	0.8073	4	0.2018			
Corrected total sum of squares	96.79	16				
Dependent variable	Regression equation					
Particle size (Y_1)	$94.18-17.90A-11.10B+4.72C+3.99AB-0.49AC+1.05BC+27.37A^2-0.02B^2-0.42C^2$					
Encapsulation efficiency (Y_2)	$84.22+1.13A+1.13B-1.64C+0.04AB+0.49AC-0.12BC-3.29A^2+0.62B^2-1.07C^2$					

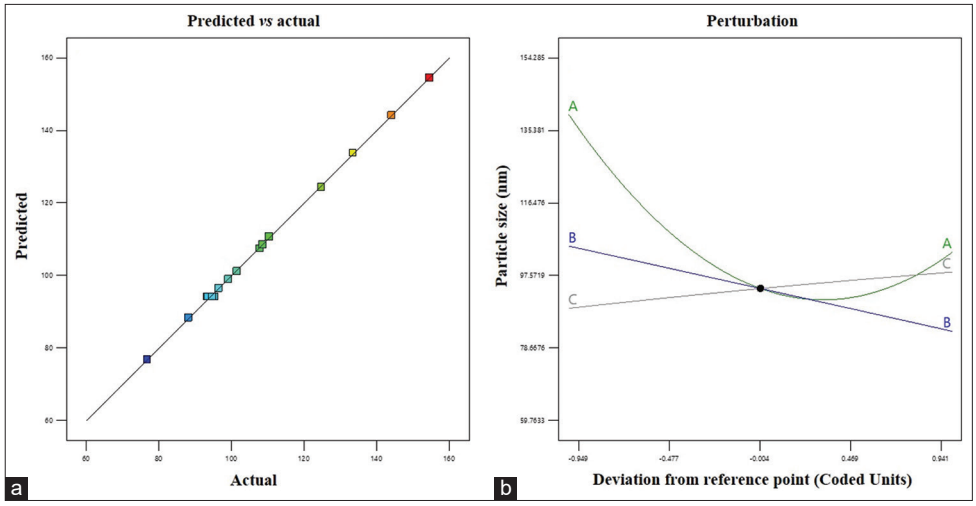

Fig. 1: Comparison between predicted and actual values on mean particle size (a); Perturbation plot displaying the effect of factors A, B, and C on particle size (b)

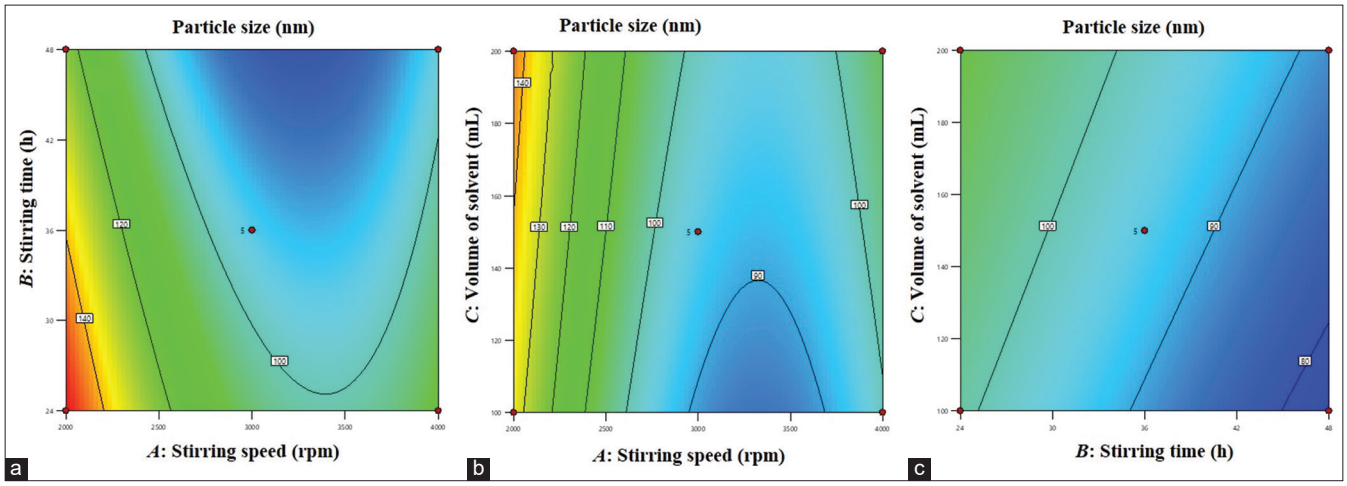

Fig. 2: (a-c) The contour plots display the interactive effect between independent variables

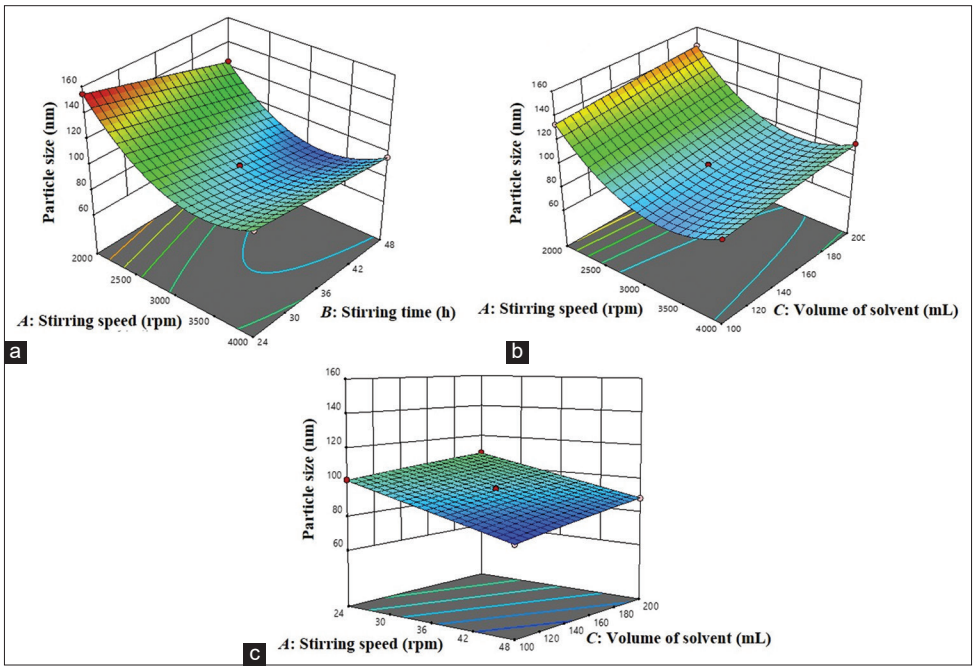

Fig. 3: (a-c) The 3D-response surface plots exhibit an interactive effect between independent variables for the dependent variable (particle size)

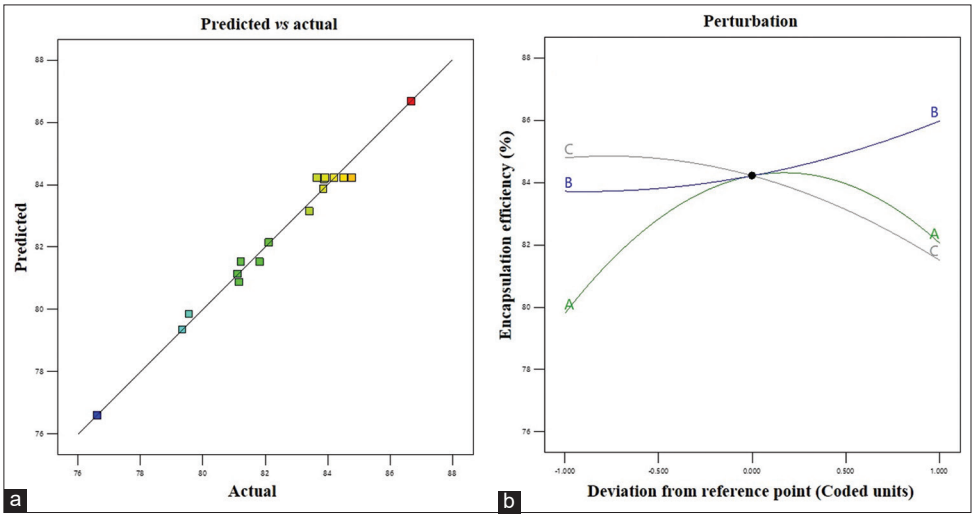

Fig. 4: Comparison between predicted and actual values-encapsulation efficiency (a); Perturbation plot showing the effect of factors A, B, and C on encapsulation efficiency (b)

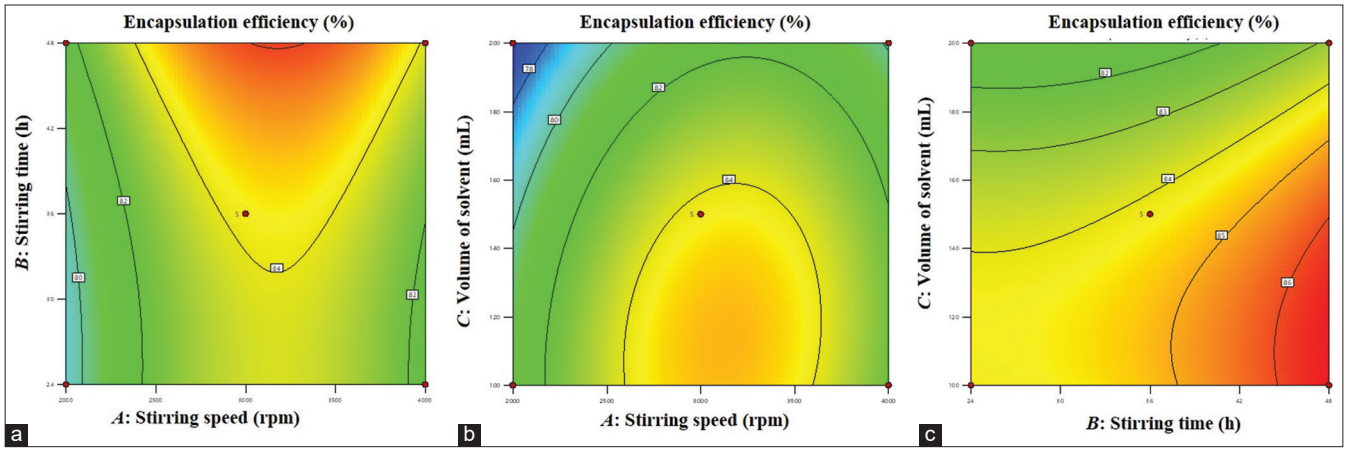

Fig. 5: (a-c) The contour plots showing the interactive effect between independent variables

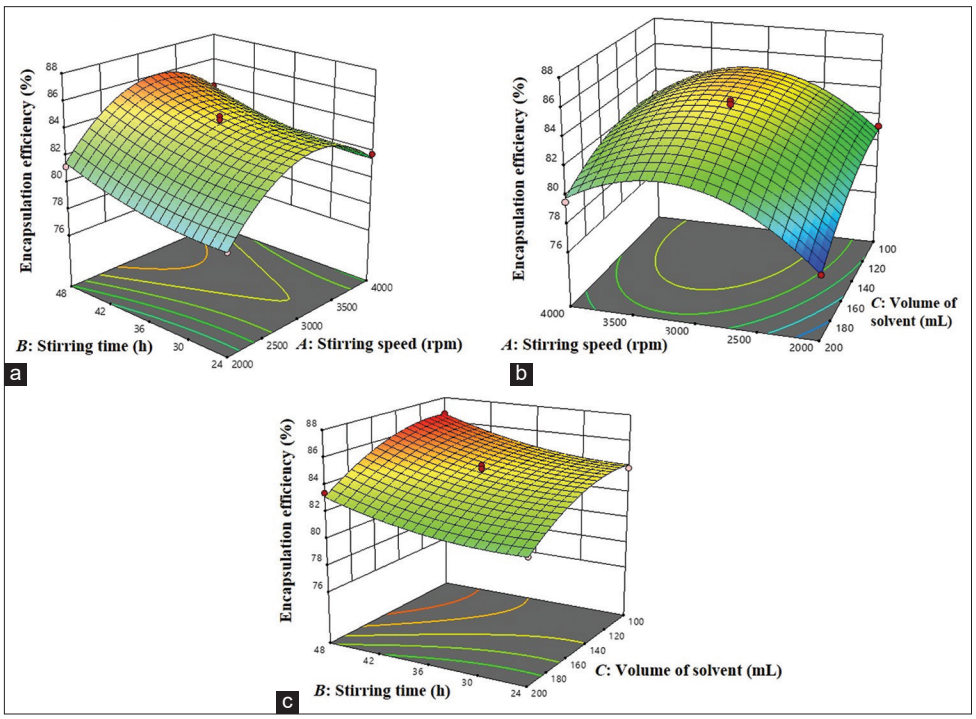

Fig. 6: (a-c) The 3D response surface plots showing the interactive effect between the independent variables for the dependent variable (encapsulation efficiency)

illustrated in the individual effects plot (Fig. 4a) and perturbation plot (Fig. 4b), which also represented the separate influences of factors A, B, and C. Figs. 5 and 6 demonstrate the combined influence of independent factors on the EE.

Optimization

The Derringer desire function (D) was employed to optimize the chosen factors that impact the response parameters. Both the results, mean particle size and EE, were converted into a desired scale. The goal function for each response parameter was determined using Y_{max} and Y_{min}, and the desirability function was combined using geometric mean and Design Expert® software for the global desirability value. The desirability function yielded an exceptional result for A: 3175 rpm, B: 48 h, and C: 110 mL, with a confirming D-value of 1.

Fig. 7 displays three-dimensional (3D) contour plots that illustrate the correlation between a response value on the Z-axis and two variables on the X- and Y-axes. The findings confirmed the effectiveness of the BBD combined with a derringer's desirability strategy in optimizing CUR-loaded *β*-CDNSs.

Characterization of plain NSs and CUR-*β*CDNSs

The examination of CUR-loaded NSs indicates that the typical particle size, as determined by laser light scattering, was around 70–80 nm, with a low polydispersity index. The particle size distribution is characterized by a single peak and has a restricted range, as seen in Table 6. A low polydispersity index indicates that the colloidal particles are uniform [25]. A suitably elevated zeta potential suggests that the complexes would exhibit stability and have a negligible inclination to agglomerate. The TEM examinations revealed that the plain NSs maintained their regular spherical form and size, even after drug encapsulation, as depicted in Fig. 8. Based on the characterization parameters as summarized in Table 3, formulation number 13 was chosen for further preparation and characterization of the optimal formulation CUR-*β*CDNSs**.**

The complexation of CUR-NSs with *β*CD further reduces the size of drug-loaded NSs with a slight increment in the polydispersity index. A minor change in the surface charge (zeta potential) of CUR-*β*CDNSs was also noted. The details about the percentage of drug loading and EE of the product are calculated and reported in Table 6. Among the three final preparations, the F2 was chosen as the optimal one for further studies as this had a smaller size (78.04 nm) with uniform distribution (PDI = 0.193), slightly high zeta potential (−29.31 mV) with increased encapsulation (88.2%) and drug loading capacity (38.8%).

The FTIR spectra of the free drug exhibited distinct peaks at the following wave numbers: 3510.56, 3421.83, 3014.84, 2850.88, 2366.74, 1627.97, 1602.90, 1510.31, 1429.30, 1280.78, 1153.47, 1026.16, 964.44, and 808.20 cm^{-1}. The plain NS exhibited a distinct peak corresponding to the imidazole bond at around 1740–1750 cm^{-1}, providing evidence for the production of *β*-CDNSs. Additional prominent peaks of NSs were seen at 2918 cm^{-1}, attributable to the stretching vibration of C–H bonds, 1418 cm^{-1}, attributable to the bending vibration of C–H bonds, and 1026 cm^{-1}, attributable to the stretching vibration of C–O bonds in primary alcohols. The FTIR spectra of physical mixtures revealed the presence of all the characteristic peaks of the medication, as well as some extra peaks corresponding to the polymers (Fig. 9) [30].

The overlay DSC thermograms of all the samples are represented in Fig. 10. The DSC curve of the pure drug (free CUR) has a distinct melting point at around 176.57°C, suggesting the drug's crystalline characteristics. The thermogram of the plain NSs exhibited exothermic peaks at around 350°C. The CUR-NSs complex had a wide exothermic peak at around 350°C. The formulation exhibited a total absence of the CUR endothermic peak. The event suggests interactions among formulation constituents, potentially indicating drug amorphization or the formation of inclusion complexes [27-29].

The X-ray diffractograms of plain CUR had distinct and strong peaks at specific 2*θ* values of 11.28, 15.92, 17.12, 19.68, 23.03, 25.8, 26.015, 27.66, 29.16, and 41.27, which confirmed the crystal structure of the medication, as shown in Fig. 11. No distinct features indicative of pure CUR were detected in the NS complexes. The lack of distinct crystalline peaks of CUR in the NS complex serves as clear evidence that the substance is enclosed within the NSs. The freeze-drying procedure results in the formation of a powdery substance with a fluffy texture and a highly porous structure. This substance loses all of its crystalline properties, as demonstrated by the X-ray powder diffraction investigation [30].

Table 6: Characteristics of plain NSs and CUR-*β*CDNSs. Data were represented as the mean of three readings with standard deviations (Mean±SD, n=3)

Sample	Particle size (nm)	PDI	Zeta potential (mV)	DL (%)	EE (%)
Plain NSs	139.78±10.47	0.191±0.025	-22.21±3.10	-	-
CUR-*β*CDNSs (F1)	83.66±9.38	0.226±0.012	-24.98±4.11	35.2±3.1	83.6±8.8
CUR-*β*CDNSs (F2)	78.04±5.94	0.193±0.006	-29.31±3.31	38.8±2.5	88.2±6.3
CUR-*β*CDNSs (F3)	80.67±8.41	0.236±0.004	-23.14±4.56	33.9±3.2	84.4±9.1

All the values were expressed in (n=3) Mean±SD

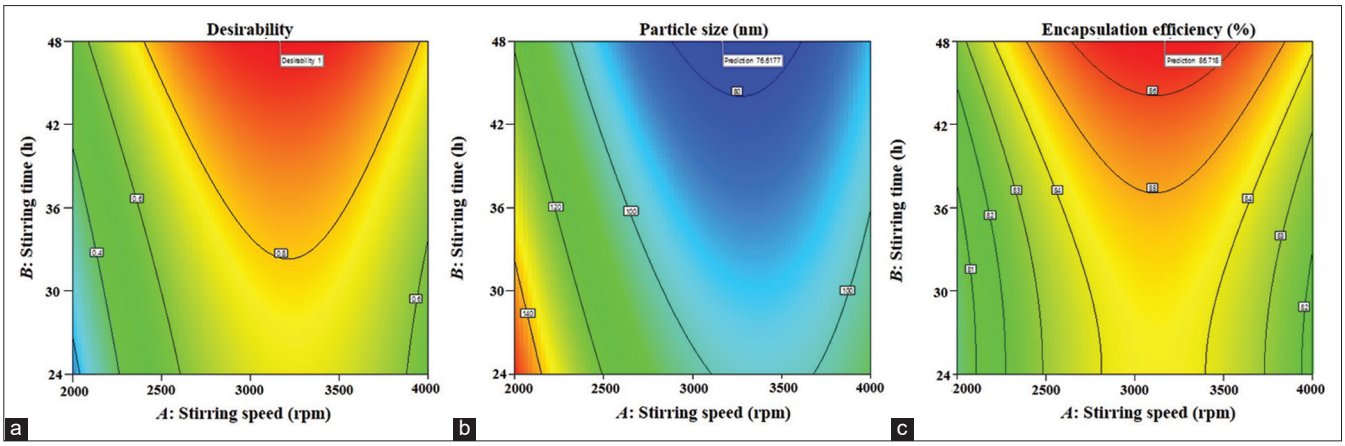

Fig. 7: The 3D contour plots showing the relationship between a response value on the Z-axis and the two variables on the X-axis and Y-axis, respectively

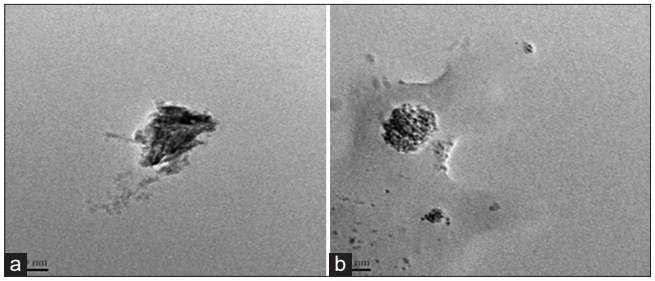

Fig. 8: The images obtained by transmission electron microscopy of the plain NSs (a) and CUR-loaded NSs (b)

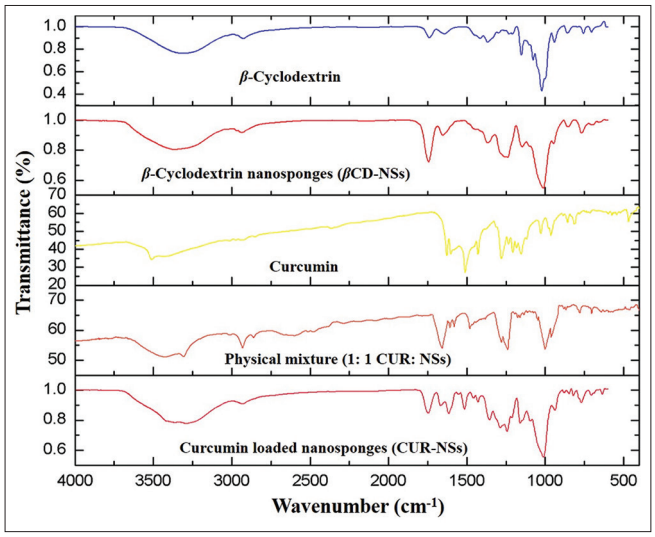

Fig. 9: The Fourier-transform infrared spectra of *β*-Cyclodextrin (*β*-CD), *β*-Cyclodextrin nanosponges (plain NSs), Curcumin (CUR), physical mixture (1:1 CUR: NSs), and curcumin-loaded nanosponges

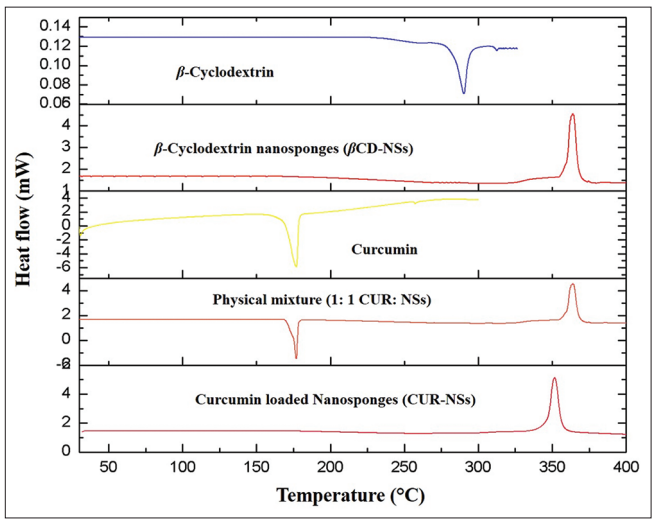

Fig. 10: Overlay differential scanning calorimetry thermograms of *β*-Cyclodextrin (*β*-CD), *β*-Cyclodextrin nanosponges (plain NSs), Curcumin (CUR), physical mixture (1:1 CUR: NSs), and curcumin-loaded nanosponges

The dissolution characteristics of free drug (CUR-suspension) and CUR-entrapped within the NSs before its complexation with *β*CD in phosphate buffer saline (pH 7.4 with 1% w/v sodium lauryl sulfate) as release medium are depicted in Fig. 12. The *in vitro* release studies demonstrated a rapid and more than 90% release of CUR from the

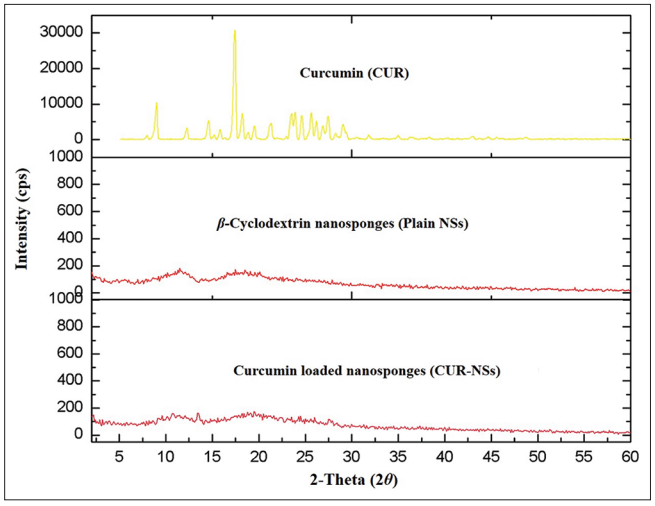

Fig. 11: The X-ray diffraction pattern of Curcumin (CUR), *β*-Cyclodextrin nanosponges (plain NSs), and curcumin-loaded nanosponges

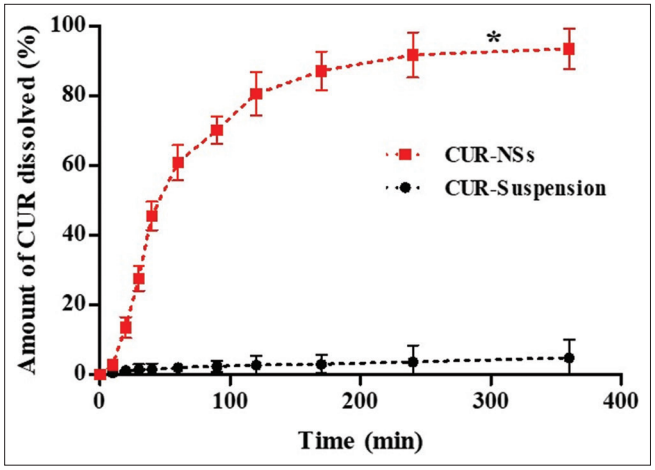

Fig. 12: *In vitro* drug release profiles of free drug (Curcumin [CUR]-suspension) and CUR-loaded nanosponges (All the values were expressed in [n=3] Mean±SD)

CUR-NSs. The pure CUR (from CUR-suspension) has only around 3% dissolution over 120 min, but CUR-entrapped NSs had a faster and burst release, with approximately 50% drug release within 30 min. The CUR-entrapped NSs rapidly diffused into the surrounding liquid, achieving a maximum CUR release of more than 85% after 120 min when added to the release medium. The rapid drug release from CUR-NSs was possibly due to the rapid diffusion of trapped CUR within the NSs as an inclusion complex. This was because, as the interaction of CUR with NSs increases, the drug solubility of poorly aqueous soluble drug (CUR) increases, and hence the rate of dissolution was increased from the CUR-NSs formulation [5].

Photodegradation and SIF stability studies

The experiment revealed that the breakdown of CUR intensifies as the duration of irradiation rises (Fig. 13a). In addition, it was shown that the breakdown of unbound CUR occurs at a quicker rate compared to CUR enclosed within NSs. This might be attributed to the robust encapsulation of CUR with NSs. The initial 30-min period saw a higher rate of CUR degradation from the formulations, possibly due to the presence of CUR on the surface of NSs [31]. Our findings are substantiated by the previous photodegradation study of resveratrol-NSs complex under UV radiation, and the drug-NSs complex was more photostable as compared to the free drug.

After the phosphate buffer (pH 7.4) stability testing, a UV-spectrophotometer measured CUR content in samples, has showed a 50% reduction in unbound CUR concentration within 24 h, but no significant decline in the entrapped forms was noted, as shown in Fig. 13b. The inclusion complex development is responsible for this phenomenon, which may be considered an effective carrier system for safeguarding the medicine from the harsh conditions of the stomach, together with the simulation of pH conditions [18]. A duration of 24 h was chosen for this study, as this was a critical and minimal stability testing time duration for the stability process, as suggested in the literature. The stability of a compound in phosphate buffer (at pH 7.4) is one of the major factors that has a positive influence on cellular interactions and permeation of drug molecules. The difficulties, such as drug leaching and recovery, can lead to the failure of cellular interactions and drug permeation. Therefore, the stability at pH 7.4 has gained increasing interest in the application of drug delivery systems and tissue engineering.

***In vitro* antioxidant activity by DPPH scavenging assay method**

The outcomes of the capacity of free CUR and CUR-*β*CDNSs complex, as compared to ascorbic acid (control), to scavenge the free radicals are illustrated in Fig. 14. The SC_{50} values of free CUR, CUR-NSs, and ascorbic acid (control) were 536.44±64.02 µg/mL, 187.48±38.55 µg/mL, and 81.16±41.62 µg/mL, respectively, which were estimated from the plots of CUR concentration against antioxidant activity. The results demonstrate an exceptional DDPH radical scavenging activity by CUR-*β*CDNSs complex as compared to free CUR, but it was inferior to the control. The DPPH radical scavenging activity was considerably boosted by 2.86-fold with the use of CUR-loaded *β*CDNSs complex. The CUR-loaded *β*CDNSs complex exhibited a significant radical-scavenging impact at a relatively low concentration, indicating its potential efficacy against DPPH radicals and to ameliorate the oxidative stress due to an excess production of reactive oxygen species (ROS).

The results indicated the enhanced efficacy of CUR from *β*CDNSs complex in reducing free radicals as compared to free CUR, which was approximately 60% at 200 µg/mL (as compared to the free CUR, i.e., around 20% at the same concentration). The increased solubility of CUR from CUR-*β*CDNSs was the reason for its improved antioxidant property as compared to free-CUR. The low value of SC_{50} categorizes improved antioxidant potency of CUR-*β*CDNSs as compared to free-CUR at the drug concentration. The CUR is a bi-functional antioxidant; it exerts antioxidant activity by scavenging the ROS (direct way) and inducing an antioxidant response (indirect way) [32]. It eases the oxidative damage by up-regulating the enzymatic activities of oxidative stress-related enzymes (SOD, CAT, and GPX) and the MAPK-Nrf2 signaling pathway. In endometriosis, reports suggest the role of CUR to reduce oxidative stress by neutralizing the free radicals, protein oxidation, and lipid peroxidation, and by down-regulating the matrix metalloproteinase-9 activity. Thus, the optimal CUR-*β*CDNSs would be helpful in alleviating the oxidative stress-related conditions and progression of endometriosis.

Evaluation of CUR-loaded *β*CDNSs hydrogel

Polymers such as Poloxamer-407 and Poloxamer-188 were used due to their non-ionic nature; these surfactants can enhance the solubility of CUR and are also employed to prevent the staining issues associated with CUR by facilitating its removal from the application site. Poloxamer-based hydrogel exhibits reduced susceptibility to dilution by vaginal fluid. Once applied, the hydrogel forms as a result of temperature rise and remains in place for an extended duration due to its mucoadhesive properties. HPMC K4M, a low viscosity grade, was used to attain an optimal mucoadhesion and prolonged drug release.

The thermoresponsive *in situ* hydrogels were synthesized using the cold technique. An optimal *in situ* hydrogel should flow freely at room temperature, allowing accurate administration and undergoing an *in situ* phase transition to form a robust gel. The optimal temperature range for vaginal thermo-reversible gels is 25–37°C, considering the human vaginal temperature of 37±2°C. The gelation temperature of a formulated solution should be between 34°C and 35°C, as below 25°C, a gel may develop at room temperature, and above 37°C, premature formula drainage.

The formulation of gel formulations relies heavily on the rheological behavior. The formulation exhibited a viscosity ranging from 6358±128.72 to 6879±221.34 cps. The gel strength is influenced by the concentration of Poloxamers and the temperature. The gel strength ranged from 12.56 to 14.12 g/cm^2 above the gelation temperature. Mucoadhesive force is crucial for *in situ* vaginal gel formation, preventing quick drainage and extending the residence period due to cohesive interactions between polymer molecules and the mucus membrane. The gel formulation exhibited a mucoadhesive strength ranging from 1356.78 to 1487.29 N/m^2.

The *in vitro* drug release profile of gel formulations is represented in Fig. 15a. The drug was released approximately 91% of the time within 60 min from CUR-*β*CDNSs in VSF, while only around 52% was released in the citrate buffer (pH 4.5). A similar release pattern of CUR was also reported from *β*CD-based NSs of CUR. The initial burst release was attributed to the presence of CUR in the matrix form and not associated with the *β*CD inclusion complex. Thereafter, sustained drug release was found, which was more in citrate buffer, which was due to the presence of CUR in the *β*CD inclusion-complex [33].

***Ex vivo* skin permeation study**

The *ex vivo* skin permeation study of CUR from CUR-*β*CDNSs hydrogels and ordinary gel was carried out through rat skin using a Franz diffusion cell. The temperature of the receptor phase was maintained at 37±2°C throughout the experiment (6 h) to simulate the normal body surface temperature. The drug permeated across the skin; versus time profiles are illustrated in Fig. 15b. During the initial time point, no drug was detected in the cases, which was due to lag time. At 1st, around 24.1% CUR was permeated from the CUR-*β*CDNSs hydrogels, while it was only 10.8% from the free CUR-hydrogel. Overall, around 1.27-fold higher amount of drug was permeated from the CUR-*β*CDNSs

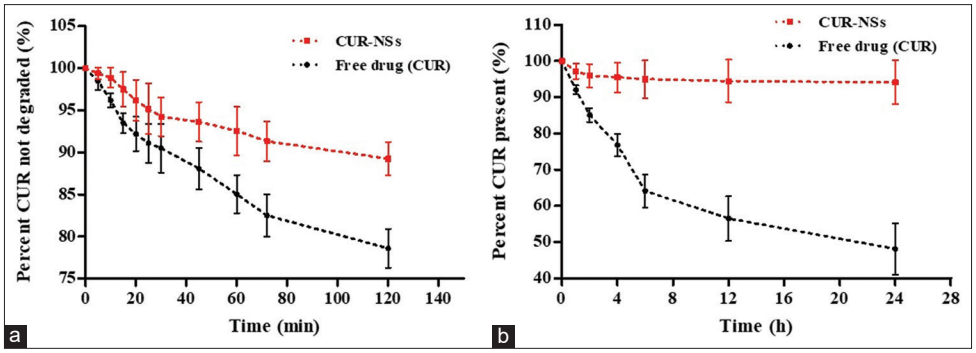

Fig. 13: Photo degradation study of free Curcumin (CUR) and CUR entrapped in the nanosponges (NSs) for 120 min (a) and the stability of free CUR and CUR-NSs in phosphate buffer (pH 7.4) at 37°C for 24 h (b); All the values were expressed in (n=3) Mean±SD

hydrogel with the flux of 9.34 µg/cm^2/h and permeability coefficient of 1.49 × 10^{-4} cm/h as compared to free drug hydrogel, where the flux and apparent permeability were 7.29 µg/cm^2/h and 1.16 × 10^{-4} cm/h, respectively.

The increased solubility of CUR from *β*CDNSs inclusion complex was the reason for its increased permeation across the rat skin. The high solubilizing and micelles-forming ability of amphiphilic co-polymers (Poloxamers 407 and Poloxamer 188) in association with the inclusion complexation of CUR with *β*CD in the case of CUR-*β*CDNSs hydrogel were the responsible factors for increased solubility of CUR [34].

Stability study

The stability of CUR-*β*CDNSshydrogel was evaluated for 6 months, stored in a stability chamber maintained at 25±1°C and 60±5% relative humidity following ICH guidelines. The appearance of the thermoresponsive hydrogel remained acceptable throughout the storage period. The other parameters, including the gelation temperature, pH, viscosity, and gel strength, were determined at specific time intervals and found to be within a range of ±5% of their initial values. The thermoresponsive CUR-*β*CDNSs hydrogel was in a solution state at the storage temperature. Similar findings were reported during the storage stability of dipivefrin hydrochloride while incorporated into poloxamers and carbopol-based thermoresponsive sol-gel system. The stability trials revealed no degradation of CUR as evidenced by the % drug content. Our results are in agreement with the previous stability reports of calcium-*β*CDNSs, resveratrol-*β*CDNSs,andmeloxicam-*β*CDNSs, where they found that the products were stable in terms of physical appearance and nature of the drug in the formulation. The detailed results and findings of the stability study are summarized in Table 7. The findings suggested that the developed formulation was stable at the mentioned storage conditions for 6 months.

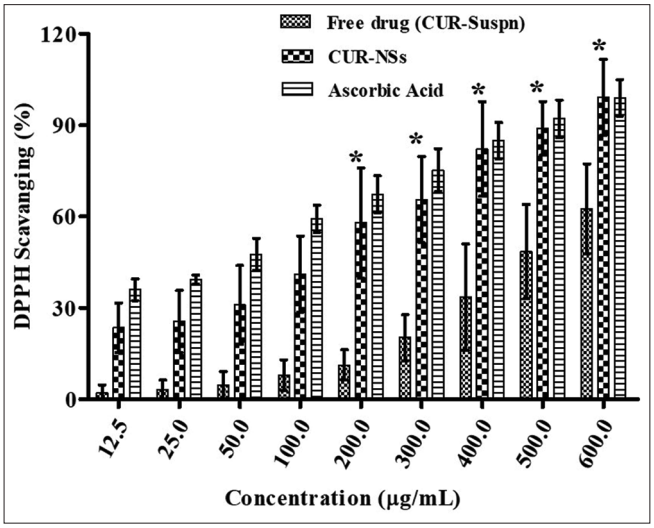

Fig. 14: The antioxidant activity of free drug (Curcumin [CUR]-Suspension) and CUR-nanosponges by DPPH free-radical scavenging assay method as compared to standard Ascorbic Acid. The data were represented as the mean of three measurements with standard deviations (mean±SD, n=3). All the values were expressed in (n=3) Mean±SD

PK analysis

The *in vivo* bioavailability studies in rabbits were conducted to examine the PKs of CUR from the developed CUR-loaded *β*CDNSs hydrogel via the transdermal route, as compared to free drug (CUR-Suspension) through the oral route. The CUR plasma concentration time profiles of CUR from the two dosage forms in rabbits are illustrated in Fig. 16, and the computed PK parameters by "PK Solver" are summarized in Table 8. The maximum plasma concentration of CUR (C_{max}) after oral administration was 87.01±6.04 ng/mL, and T_{max} was 2.5h. For the CUR-*β*CDNSshydrogel, the C_{max} was 80.09±5.29 ng/mL (slightly less than that of oral), and T_{max} was 6h (2.4-fold), which was significantly higher ($p<0.05$) as compared to the CUR-oral suspension. This obvious difference in the T_{max} was due to the barrier property of the stratum corneum as well as the sustained release of CUR from the *β*CDNSs complex in the hydrogel. In contrast, the CUR suspension administered by oral route served as a conventional immediate-release dosage form and hence had a lower T_{max} (2.5 h). Around 1.59-fold increased $t_{1/2}$ was noted in the case of *β*CDNSs complex-treated group as compared to the CUR suspension-treated group, which was due to the sustained and prolonged release of CUR from the hydrogel through the transdermal route.

The hydrogel formulation had a lag time (T_{lag}) of 1.5 h, which was anticipated as the natural defensive mechanism of the skin structures might delay the drug penetration across the skin when the CUR-*β*CDNSshydrogel was applied topically. Around 2-fold higher ($p<0.05$) $AUC_{0\text{-}24,}$ $AUC_{0\text{-}inf,}$ and $AUMC_{0\text{-}inf}$ of the CUR were noted from the transdermal application of CUR-*β*CDNSs hydrogel as compared to oral CUR suspension. Around 2.03 times increased $MRT_{0\text{-}inf}$ of CUR was found from the transdermal route as compared to the orally administered counter formulation. The results are in agreement with a study where a significantly higher bioavailability of CUR was reported from CUR-*β*CD inclusion complex-based nanoparticles as compared to free-CUR. The reasonably inferior PKs of orally administered CUR suspension were due to its relatively rapid clearance (2.22 times faster) from the systemic circulation [35].

These findings aligned with the *ex vivo* permeation of CUR, where *β*CDNSs hydrogel had 1.27-fold increased CUR permeability as compared to the conventional CUR hydrogel. Apart from the strong mucoadhesive

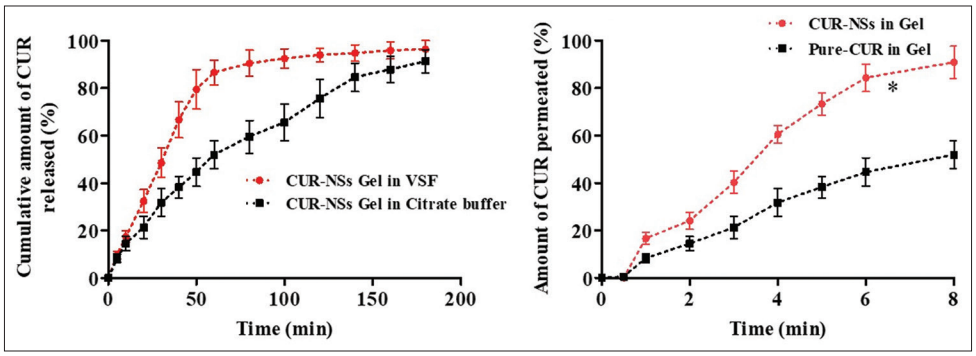

Fig. 15: *In vitro* release profile of Curcumin (CUR) from CUR-*β*-Cyclodextrin nanosponges (*β*CDNSs) hydrogels at two different release media (a) and ex vivo permeation of CUR from CUR-NSs hydrogels as compared to pure-CUR in gel (b). Where "*" represents the significantly enhanced ($p<0.05$) permeation of CUR from NSs gel as compared to Pure-CUR gel. All the values were expressed in (n=3) Mean±SD

property of HPMC (K4M), the improved PKs of CUR by CUR-*β*CDNSs hydrogel was also attributed to the solubilizing and micelle-forming properties of the amphiphilic Poloxamers in association with the increased solubility and permeability of *β*CD-based inclusion complex of NSs. This was also supported by the plasma clearance (Cl/F) of CUR, which was 2.22 times slower than that of the orally administered free CUR-suspension. Therefore, CUR-*β*CDNSs can be a promising alternative to conventional CUR suspension with enhanced bioavailability of CUR for efficient treatment of endometriosis.

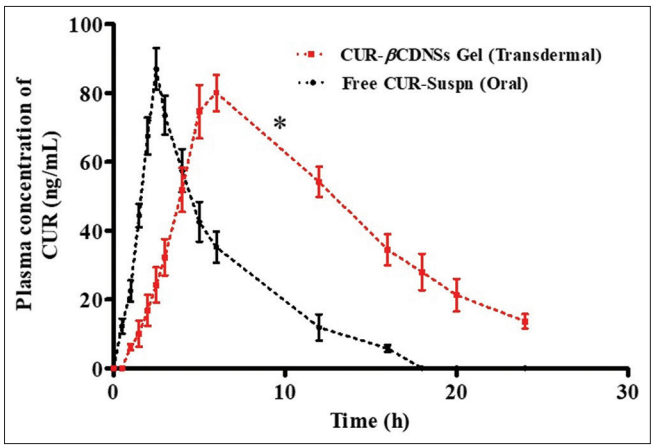

Fig. 16: Plasma concentration profiles of Curcumin (CUR) after oral administration of free drug (CUR-Suspension) and transdermal application of CUR, CUR-*β*-Cyclodextrin nanosponges (*β*CDNSs) hydrogel in rabbits. Results were represented as the mean of three measurements with standard deviations (mean±SD, n=6). Where "*" represents the significantly enhanced ($p<0.05$) pharmacokinetics of CUR from CUR-*β*CDNSs hydrogel when applied via transdermal route as compared to oral administration of free drug suspension (CUR-Suspension). All the values were expressed in (n=6) Mean±SD

Histopathology study

The increased stromal vessel density and well-preserved epithelium in control mice (Fig. 17a) contrasted with the leukocyte infiltration and fibrosis that characterized the endometriosis group (Fig. 17b). The normal gel (CUR-pure in gel base) treatment did not show significant improvement (Fig. 17c). However, the treatment with CUR-loaded NSs nanogel significantly ameliorated these pathological features (Fig. 17d). The standard drug danozol-treated group was represented as a reference (Fig. 17e). This finding is consistent with a report showing that amygdalin treatment considerably reduces the pathological score in endometriosis. In the surgically induced endometriosis group, we observed significant changes in endometriosis lesions. Destruction of the endometrium was more evident in the columnar epithelial layer and glands. The prominent hemorrhage, vascular congestion, necrosis, inflammatory cell infiltration, cystically dilated glands, and significant blood cell accumulation in the lumen of endometrial lesions were detected in the endometrial lesion layers. All histological parameters were significantly improved after CUR-loaded *β*CDNSs hydrogel administration. These histological examinations of the mouse endometrium and related findings proved that the CUR-*β*CDNSs hydrogel could preserve the changes as compared to the conventional hydrogel, where free CUR was directly incorporated into the Poloxamer-based hydrogel base.

The results of the present investigation are in line with the previous reports where a CUR-hydrogel, which was liquid at room temperature, underwent gelation at normal physiological temperature after being injected into the rat's uterine cavity, reducing fibronectin deposition

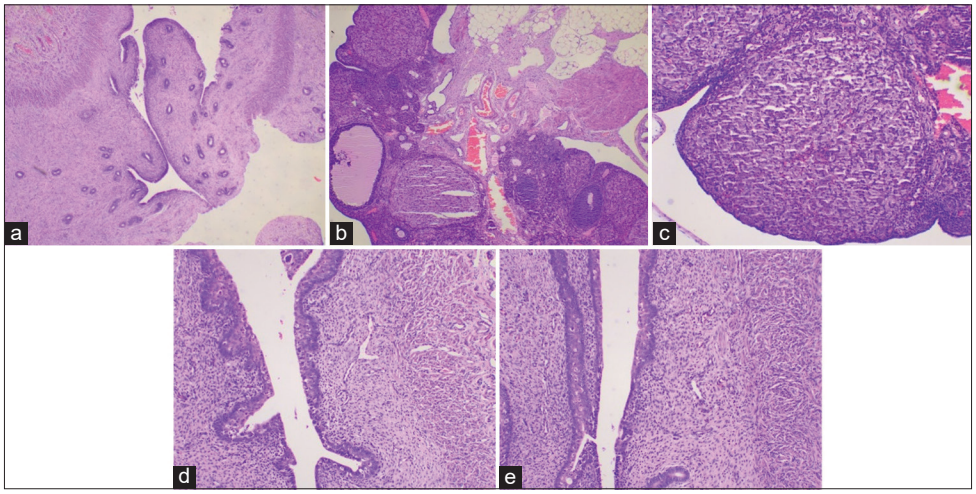

Fig. 17: The histopathology study of endometriosis. Where the normal control group (a), endometriosis control group (b), normal hydrogel (Curcumin [CUR] in gel base) treated group (c), CUR-*β*-Cyclodextrin nanosponges hydrogel treated group (d), and standard drug (danozol) treated group (e)

Table 7: Stability of CUR-*β*CDNSs hydrogel formulation for 6 months' storage. Results were represented as the mean of three measurements with standard deviations (mean±SD, n=3)

Parameter	0 days	15th day	30th day	60th day	120th day	180th day
Appearance	Acceptable	Acceptable	Acceptable	Acceptable	Acceptable	Acceptable
Gelation temp	34.4°C	34.8°C	33.9°C	34.2°C	33.6°C	33.8°C
pH	4.54±0.38	4.87±0.12	4.69±0.27	4.46±0.32	4.72±0.42	4.82±0.54
Viscosity (cps)	6684±118.5	6712±212.3	6978±187.3	6548±312.5	6743±212.6	6897±179.54
Gelstrength (gm/cm^2)	13.76±0.78	13.18±0.54	13.68±0.86	13.92±0.82	14.12±0.46	13.99±0.38
%Drug content	96.56±4.38	95.78±3.56	95.52±4.76	95.45±5.08	95.15±6.05	94.49±4.85

All the values were expressed in (n=3) Mean±SD

Table 8: Pharmacokinetic parameters of CUR after oral administration of free drug (CUR-Suspension) and transdermal application of CUR-*β*CDNSs hydrogel in rabbits. Results were represented as the mean of three measurements with standard deviations (mean±SD, n=3)

Pharmacokinetic parameters	Free CUR (CUR-suspension)	CUR-*β*CDNSs hydrogel	Fold-improvement
$t_{1/2}$ (h)	3.71±0.31	5.89±0.35	1.59
T_{max} (h)	2.5±0.0	6.0±0.0	2.40
C_{max} (ng/mL)	87.01±6.04	80.09±5.29	0.92
T_{lag} (h)	0.0±0.0	1.5±0.0	-
$AUC_{0\text{-}24\ h}$ (ng/mL.h)	466.04±62.78	982.21±106.76	2.11
$AUC_{0\text{-}inf}$ (ng/mL.h)	496.97±70.57	1097.68±117.61	2.21
$MRT_{0\text{-}inf}$ (h)	6.27±0.35	12.74±0.08	2.03
Vz/F (mL)*	676.58±42.61	490.11±79.58	1.38
Cl/F (mL/h)**	127.48±18.17	57.37±6.01	2.22

Where "Vz/F *" represents the apparent volume of distribution of the central compartment after oral administration of CUR-Suspension and transdermal application of CUR-*β*CDNSs. While "(Cl/F) **" represents the apparent clearance. All the values were expressed in (n=3) Mean±SD

and augmenting the endometrial recovery [36]. The improved activity of CUR while in *β*CDNSs inclusion complex was due to the higher drug solubilization, which could remarkably show its intrinsic antioxidant, anti-inflammatory, and anti-fibrosis properties for ameliorating the abnormal fibrosis in the condition of induced endometriosis.

The destruction of the endometrium, necrosis, and inflammatory cell infiltration is more evident in endometriosis-induced groups. The treated groups with normal hydrogel and CUR-*β*CDNSs hydrogel preserved the pathological changes significantly, which was confirmed by well-preserved epithelium. The standard drug danozol was used for reference.

CONCLUSION

The CUR-*β*CDNSs were synthesized with favorable properties such as particle size distribution, heat resistance, and porous structure for drug encapsulation, effectively entrapping CUR using response surface methods. The optimized conditions for the NS system, including temperature, duration, stirring speed, and solvent, were achieved through an extensive study of drug-loaded nanoparticles using various techniques. Such as particle size measurement, FTIR, DSC, and XRD. The CUR complexed with the nano-synthesized NSs forms an amorphous drug complex, promising a woman-friendly, long-lasting, and biocompatible intravaginal gel for endometriosis treatment, but preclinical research is needed. The findings contribute to the advancement of drug delivery systems, particularly for hydrophilic medications, and offer potential benefits for improved patient adherence and pharmaceutical bioavailability. It could take longer for *in vivo* research in larger populations and clinical studies to confirm the effectiveness of CUR-*β*CDNSs hydrogel as a medicine for the treatment of endometriosis.

ACKNOWLEDGMENT

The authors express their gratitude to the administration and staff of DIT University, Dehradun, Uttarakhand, India, and St Mary's College of Pharmacy, Secunderabad, Telangana, India, for their valuable support in allowing the research. The students are appreciative of the assistance and motivation they have received throughout their time at this establishment.

AUTHORS CONTRIBUTION

Abhini Ummangal Balan conducted comprehensive research and authored the manuscript. Bhavna Kumar, Gurusamy Mariappan played a key role in analyzing the complete dataset and provided guidance and oversight throughout the project's duration.

CONFLICTS OF INTEREST

The authors declare that they have no competing interests.

AUTHOR FUNDING

We have not received any funding.

REFERENCES

1. Pawar S, Shende P, Trotta F. Diversity of *β*-cyclodextrin-based nanosponges for transformation of actives. Int J Pharm. 2019;565:333-50. doi: 10.1016/j.ijpharm.2019.05.015, PMID 31082468
2. Selvamuthukumar S, Anandam S, Krishnamoorthy K, Rajappan M. Nanosponges: A novel class of drug delivery system-review. J Pharm Pharm Sci. 2012;15(1):103-11. doi: 10.18433/j3k308, PMID 22365092
3. Muralikrishna P, Babu AK, Mamatha P. Formulation and optimization of ceritinib loaded nanobubbles by Box-Behnken design. Int J App Pharm. 2022 Apr;14(4):219-26. doi: 10.22159/ijap.2022v14i4.44388
4. Konda M, Sampathi S. QbD approach for the development of capsaicin-loaded stearic acid-grafted chitosan polymeric micelles. Int J App Pharm. 2023 Apr;15(4):131-42. doi: 10.22159/ijap.2023v15i4.48101
5. Tejashri G, Amrita B, Darshana J. Cyclodextrin based nanosponges for pharmaceutical use: A review. Acta Pharm. 2013 Sep;63(3):335-58. doi: 10.2478/acph-2013-0021, PMID 24152895
6. Venuti V, Rossi B, Mele A, Melone L, Punta C, Majolino D, *et al*. Tuning structural parameters for the optimization of drug delivery performance of cyclodextrin-based nanosponges. Expert Opin Drug Deliv. 2017 Mar;14(3):331-40. doi: 10.1080/17425247.2016.1215301, PMID 27449474
7. Vij M, Dand N, Kumar L, Wadhwa P, Wani SU, Mahdi WA, *et al*. Optimisation of a greener-approach for the synthesis of cyclodextrin-based nanosponges for the solubility enhancement of domperidone, a BCS Class II drug. Pharmaceuticals (Basel). 2023 Apr 10;16(4):567. doi: 10.3390/ph16040567, PMID 37111324
8. Atchaya J, Girigoswami A, Girigoswami K. Versatile applications of nanosponges in biomedical field: A glimpse on SARS-CoV-2 management. Bionanoscience. 2022;12(3):1018-31. doi: 10.1007/s12668-022-01000-1, PMID 35755139
9. Chary SS, Bhikshapathi DV, Vamsi NM, Kumar JP. Optimizing entrectinib nanosuspension: Quality by design for enhanced oral bioavailability and minimized fast-fed variability. Bionanosciencе. 2024;14(4):4551-69. doi: 10.1007/s12668-024-01462-5
10. Aparna A, Kumar YS, Bhikshapathi DV. Formulation and *in vivo* evaluation of ticagrelor self-nanoemulsifying drug delivery systems. Pharm Nanotechnol. 2021;9(1):61-9. doi: 10.2174/2211738508666200708150151, PMID 32640972
11. Ji X, Li Z, Wang M, Yuan Z, Jin L. Response surface methodology approach to optimize parameters for coagulation process using polyaluminum chloride (PAC). Water. 2024;16(11):1470. doi: 10.3390/w16111470
12. Singireddy A, Rani Pedireddi SR, Nimmagadda S, Subramanian S. Beneficial effects of microwave-assisted heating versus conventional heating in synthesis of cyclodextrin-based nanosponges. Mater Today Proc. 2016;3(10):3951-9. doi: 10.1016/j.matpr.2016.11.055
13. Trotta F, Zanetti M, Cavalli R. Cyclodextrin-based nanosponges as drug carriers. Beilstein J Org Chem. 2012;8:2091-9. doi: 10.3762/bjoc.8.235, PMID 23243470
14. Kalam MA. Development of chitosan nanoparticles coated with hyaluronic acid for topical ocular delivery of dexamethasone. Int J Biol Macromol. 2016;89:127-36. doi: 10.1016/j.ijbiomac.2016.04.070, PMID 27126165

15. Gao W, Zhang Y, Zhang Q, Zhang L. Nanoparticle-hydrogel: A hybrid biomaterial system for localized drug delivery. Ann Biomed Eng. 2016;44(6):2049-61. doi: 10.1007/s10439-016-1583-9, PMID 26951462
16. Moin A, Roohi NK, Rizvi SM, Ashraf SA, Siddiqui AJ, Patel M, *et al*. Design and formulation of polymeric nanosponge tablets with enhanced solubility for combination therapy. RSC Adv. 2020;10(57):34869-84. doi: 10.1039/d0ra06611g, PMID 35514416
17. Zhang Y, Sun Y, Yang X, Hilborn J, Heerschap A, Ossipov DA. Injectable *in situ* forming hybrid iron oxide-hyaluronic acid hydrogel for magnetic resonance imaging and drug delivery. Macromol Biosci. 2014;14(9):1249-59. doi: 10.1002/mabi.201400117, PMID 24863175
18. Bitar R, Cools P, De Geyter N, Morent R. Acrylic acid plasma polymerization for biomedical use. Appl Surf Sci. 2018;448:168-85. doi: 10.1016/j.apsusc.2018.04.129
19. Tietz K, Klein S. Simulated genital tract fluids and their applicability in drug release/dissolution testing of vaginal dosage forms. Dissolution Technol. 2018;25(3):40-51. doi: 10.14227/dt250318p40
20. Abushammala IM, Mohammed Mqat B, Mohammed Hamdan A. Effect of curcumin at various doses on the pharmacokinetic profile of tacrolimus in healthy rabbits. Iraqi J Pharm Sci. 2022;31(1):246-50. doi: 10.31351/vol31iss1pp246-250
21. Fonseca-Santos B, Gremião MP, Chorilli M. A simple reversed phase high-performance liquid chromatography (HPLC) method for determination of *in situ* gelling curcumin-loaded liquid crystals in in vitro performance tests. Arab J Chem. 2017;10(7):1029-37. doi: 10.1016/j.arabjc.2016.01.014
22. Burns KA, Pearson AM, Slack JL, Por ED, Scribner AN, Eti NA, *et al.* Endometriosis in the mouse: Challenges and progress toward a 'best fit' murine model. Front Physiol. 2021;12:806574. doi: 10.3389/fphys.2021.806574, PMID 35095566
23. Hossain S, Islam A, Tasnim F, Hossen F, E-Zahan K, Asraf A. Antimicrobial, antioxidant and cytotoxicity study of Cu(II), Zn(II), Ni(II), and Zr(IV) complexes containing O, N donor Schiff base ligand. Int J Chem Res. 2024 Oct;8(4):1-11. doi: 10.22159/ijcr.2024v8i4.231
24. Mashaqbeh H, Obaidat R, Al-Shar'I N. Evaluation and characterization of curcumin-*β*-cyclodextrin and cyclodextrin-based nanosponge inclusion complexation. Polymers (Basel). 2021;13(23):4073. doi: 10.3390/polym13234073, PMID 34883577
25. Chary SS, Bhikshapathi DV, Rajesham VV, Penakalapati SR, Sandhya P, Sadasivam RK. Formulation and evaluation of nano formulation of BTK inhibitor by Box-Behnken design and high-pressure homogenization for enhanced bioavailability and reducing the effects of food. Int J App Pharm. 2025;17(4):521-8. doi: 10.22159/ijap.2025v17i4.54079
26. Phalak SD, Bodke V, Yadav R, Pandav S, Ranaware M. A systematic review on nano drug delivery system: Solid lipid nanoparticles (SLN). Int J Curr Pharm Res. 2024 Jan;16(1):10-20. doi: 10.22159/ijcpr.2024v16i1.4020
27. Bayer IS. Controlled drug release from nanoengineered polysaccharides. Pharmaceutics. 2023;15(5):1364. doi: 10.3390/pharmaceutics15051364, PMID 37242606
28. Biswas J, Sinha D, Mukherjee S, Roy S, Siddiqi M, Roy M. Curcumin protects DNA damage in a chronically arsenic-exposed population of West Bengal. Hum Exp Toxicol. 2010;29(6):513-24. doi: 10.1177/0960327109359020, PMID 20056736
29. Pedireddi S, Singireddy A, Varma MM, Jayanthi VR. Differential properties of nanoporousnanosponges prepared from *β*-cyclodextrin and 2-hydroxypropyl *β*-cyclodextrin. Adv Sci Eng Med. 2019;11(9):823-35. doi: 10.1166/asem.2019.2423
30. Gharakhloo M, Sadjadi S, Rezaeetabar M, Askari F, Rahimi A. Cyclodextrin-based nanosponges for improving solubility and sustainable release of curcumin. ChemistrySelect. 2020;5(5):1734-8. doi: 10.1002/slct.201904007
31. Garg A, Lai WC, Chopra H, Agrawal R, Singh T, Chaudhary R, *et al*. Nanosponge: A promising and intriguing strategy in medical and pharmaceutical science. Heliyon. 2024;10(1):e23303. doi: 10.1016/j.heliyon.2023.e23303, PMID 38163139
32. Chandana L, Bhikshapathi D. Free radical scavenging activity of *Pleurotus ostreatus* against CCL_4-induced hepatic damage in Wistar rats. Int J Pharm Pharm Sci. 2023 Dec;15(12):17-22. doi: 10.22159/ijpps.2023v15i12.49478
33. Möller K, Macaulay B, Bein T. Curcumin encapsulated in crosslinked cyclodextrin nanoparticles enables immediate inhibition of cell growth and efficient killing of cancer cells. Nanomaterials (Basel). 2021;11(2):489. doi: 10.3390/nano11020489, PMID 33672006
34. Chandana L, Bhikshapathi DV. Ethnopharmacological investigation of *Pleurotus ostreatus* for anti-oxidative and anti-inflammatory activity in experimental animals. Asian J Pharm Clin Res. 2024 Apr;17(4):37-41. doi: 10.22159/ajpcr.2024.v17i4.49533
35. Jiang L, Xia N, Wang F, Xie C, Ye R, Tang H, *et al*. Preparation and characterization of curcumin/*β*-cyclodextrin nanoparticles by nanoprecipitation to improve the stability and bioavailability of curcumin. LWT. 2022;171:114149. doi: 10.1016/j.lwt.2022.114149
36. Zhang W, He Y, Chu Y, Zhai Y, Qian S, Wang X, *et al*. Amorphous curcumin-based hydrogels to reduce the incidence of post-surgical intrauterine adhesions. Regen Biomater. 2024;11:rbae043. doi: 10.1093/rb/rbae043, PMID 38779348